Hindawi
Advances in Materials Science and Engineering
Volume 2020, Article ID 7872815, 13 pages
https://doi.org/10.1155/2020/7872815

Research Article

Notch Effect on Plastic Deformation of Metallic Glass: A Numerical Study by Revised Free-Volume Theory

J. F. Yan,[1,2] **W. J. Meng**,[1,3] **Z. Chen**,[1] **H. Guo**,[1] **and X. G. Yan**[1]

[1]*School of Mechanical Engineering, Taiyuan University of Science and Technology, Taiyuan 030024, China*
[2]*CIECC Engineering Management Consulting Co.,Ltd., Beijing 100048, China*
[3]*School of Mechanical Engineering, Shanxi Institute of Energy, Taiyuan 030600, China*

Correspondence should be addressed to J. F. Yan; paulyan@stu.tyust.edu.cn and W. J. Meng; tyustmwj@126.com

Received 30 March 2020; Revised 19 June 2020; Accepted 25 June 2020; Published 18 July 2020

Academic Editor: Dimitrios E. Manolakos

By means of a revised free-volume theory, the notch effect on metallic glass was systematically investigated by the numerical method. Simulations on specimens without notches demonstrated that the parameters being determined in this work could reasonably describe the strength asymmetry of tension and compression. Moreover, four samples with different notches were used to numerically investigate the notch effect on global strength and plasticity. A better agreement could also be achieved between current simulations with existing experimental results, compared with another free-volume model. Combined with the free-volume distribution during deformation process, it was proven that the intersection of two major shear bands is the cause for the strength and plasticity enhancement found in sample with two symmetric notches. Besides, strength asymmetry between tension and compression was also found for notched samples. Compressive strengths are accordingly higher than tensile ones. Moreover, with the augment of the aspect ratio, the plasticity for specimens with two symmetric notches was found to increase firstly and then decrease afterwards.

1. Introduction

Recently, metallic glass has received loads of attentions because of its unique properties such as high strength, large elastic limit, and high hardness [1–3]. However, the vital shortcoming of monolithic metallic glass is the fast shear banding process, and it seldom exhibits noticeable plasticity once its yield strength has been reached. Although some scholars claimed that its plasticity could be enhanced by tuning structural or spatial heterogeneities [4–6], the low ductility is still its main weakness, which limits its wide application in engineering. Therefore, many investigations have been dedicated to this field with the purpose of improving its ductility. It is proven that installing multiple stress states could effectively improve the global plasticity of metallic glasses [7–13]. Among these works, it was found that installing two symmetric notches could largely enhance the compressive plasticity [7]. It has been recognized that the interaction of two major shear bands is the key for the plasticity argument, which could confine specimens without fracturing rapidly along one shear band.

On the contrary, how to understand the intrinsic mechanism behind the existing findings is very crucial to advance the deformation mechanism of metallic glasses. From the viewpoints of technology, the finite element model (FEM) is an effective way of understanding and revealing different mechanisms, and it is very convenient and economical since the computer ability is improving and results obtained by FEM could be vividly compared and validated by relevant experiments. In general, free-volume theory [14] has been accepted as a good candidate to simulate the onset of shear band initiation and propagation. Gao [15] developed a computational framework, which incorporated the free-volume theory [14] into FEM, and it was concluded that the shear banding process could be described by free-volume aggregation, which was localized and shaped like the shear band morphology obtained in experiment. Besides, Jiang [16, 17] investigated shear banding process when different notches and test

conditions were arranged, and it was found that simulated results were consistent with experimental findings. Furthermore, since the hydrostatic stress is very significant especially when the sample is deformed in complex stress states, several models accounting for hydrostatic stress were proposed to simulate the shear band propagation process [18–22]. For instance, Thamburaja and Ekambaram [18, 19] proposed a finite-deformation-based model, in which the hydrostatic stress was considered. Simulated results were found to precisely imitate strain localization (shear banding process) in metallic glass. Besides, Rao et al. [20] developed a constitutive model which can describe the failure characteristics of metallic glass under different stress states by incorporating stress triaxiality. Moreover, Zhao et al. [21] raised a micromechanics-based model to depict the shear band evolution during tensile and compressive loadings and the tension and compression asymmetry was reasonably interpreted.

Although a few models have been developed to analyze the shear banding process under complex stress states, few approaches have been reported on the notch effect of metallic glass when hydrostatic stress is considered. Since notch could result in stress concentration leading to stress triaxiality, it is necessary to investigate the shear banding process in metallic glass when different notches are installed and eventually to understand dependence of notch configuration on the global plasticity. Therefore, according to a recent constitutive law considering hydrostatic stress [21], systematic simulations are performed to understand the dependence of the global plasticity on the notch configurations and geometry by means of a user material subroutine (UMAT) in ABAQUS software. It proves again that the intersection of two symmetric notches could effectively postpone the fast shear banding process in sample so that the global plasticity is expected to be enhanced. On the contrary, for specimens with only one notch, two unsymmetric notches as well as one hole, strain is localized along one shear band because of the absence of two shear bands interaction. Therefore, the related plasticity is very limited. It is anticipated that the current work could broaden the understanding of deformation mechanism for metallic glass under complex stress states.

2. Constitutive Laws considering Hydrostatic Stress Contribution

Since there is no dislocation in metallic glasses, shear band initiation and localization is the sole mechanism governing the deformation behavior. From the macroscopic viewpoints [23], the plasticity difference under tension and compression could be attributed to the loading mode and normal stress. Under compression, because of the shrink effect caused by compression, the specimen displays some plasticity before fracture. From the microscopic level, shear band deformation is believed to be dependent on the local structural disorder [14], which could be numerically built up by free-volume theory [14, 15]. In fact, the free volume is a mathematical measure of the departure from the ideally ordered structure and believed as the difference between the averaged atomic volume and that in the ideally ordered structure [14, 15]. In terms of the contribution of hydrostatic stress, it was concluded that the free volume localization is prone to take place under tensile loading because the tensile hydrostatic stress is in favor of making shear band localized [21]. However, under compression, the compressive hydrostatic stress could confine the aggregation of free volume, delaying the onset of fast shear banding process [21]. Therefore, by the constitutive law proposed by Zhao et al. [21], the net rate of free-volume increase is [21]

$$\frac{\partial \overline{v_f}}{\partial t} = \frac{\xi\,\Omega\,(1-2v)}{E}\,\frac{\partial \sigma_{kk}}{\partial t} + v^* f\,\exp\left[-\frac{\alpha v^*}{\overline{v_f}}\right]\exp\left[-\frac{\Delta G^m}{k_B T}\right] \times \left\{\frac{2\alpha k_B T}{\overline{v_f} C_{eff}}\left(\cosh\left(\frac{\tau\,\Omega}{2k_B T}\right)-1\right)-\frac{1}{n_D}\right\}, \tag{1}$$

where f stands for the frequency of atomic vibration, α is a geometrical coefficient of order 1, v^* is the critical volume (hard-sphere volume of an atom), $\overline{v_f}$ is the average free volume per atom, Ω is the atomic volume, E and v are elastic modulus and Poisson's ratio, ΔG^m is the activation energy, τ represents for the shear stress, k_B is the Boltzmann constant and T is the absolute temperature, C_{eff} is the effective elastic stress, typically we have $C_{\text{eff}} = E/3(1-v)$, n_D is the number of atomic jumps needed to annihilate a free volume equal to v^* and is usually taken as 3 [14–17, 21], σ_{kk} is the hydrostatic stress term [21], and ξ is a factor which characterizes the response of free volume increment induced by hydrostatic stress for individual material [21]. The ξ value could be obtained by comparing tensile and compressive strength via the finite element method and experimental results [21].

Based on the J_2 theory, under small deformation scheme, the total strain rate $\dot{\varepsilon}_{ij}$ accounting for the term of hydrostatic stress can be decomposed into elastic part $\dot{\varepsilon}^e_{ij}$, plastic part $\dot{\varepsilon}^p_{ij}$, and hydrostatic stress induced strain rate $\dot{\varepsilon}^h_{ij}$:

$$\dot{\varepsilon}_{ij} = \dot{\varepsilon}^e_{ij} + \dot{\varepsilon}^p_{ij} + \dot{\varepsilon}^h_{ij}. \tag{2}$$

The elastic part $\dot{\varepsilon}^e_{ij}$ is

$$\dot{\varepsilon}^e_{ij} = \frac{1+v}{E}\left(\dot{\sigma}_{ij} - \frac{v}{1+v}\dot{\sigma}_{kk}\,\delta_{ij}\right). \tag{3}$$

Equation (3) is the conventional Hooke's law for isotropic solids in terms of the isotropy of metallic glass [15]. Then, one can obtain

$$\sigma_e = \sqrt{\frac{3}{2}S_{ij}S_{ij}}, \qquad S_{ij} = \sigma_{ij} - \frac{\sigma_{kk}\delta_{ij}}{3}, \tag{4}$$

where σ_e is the effective stress and S_{ij} is the deviatoric stress. By means of the characteristic time scale $t^* = t f^{-1} \exp(\Delta G^m/k_B T)$, the plastic part, i.e., the flow equation $\dot{\varepsilon}^p_{ij}$ in equation (2) and

free-volume evolution equation (equation (1)) could be deduced as [21, 24]

$$\dot{\varepsilon}_{ij}^{p} = \exp\left(-\frac{1}{v_f}\right)\sinh\left(\frac{\sigma_e}{\sigma_0}\right)\frac{S_{ij}}{\sigma_e}, \tag{5}$$

$$\begin{aligned}\dot{v}_f &= \frac{\xi\,\Omega\,(1-2v)}{\alpha v^* E}\dot{\sigma}_{kk} + \frac{1}{\alpha}\exp\left(-\frac{1}{v_f}\right) \\ &\times \left\{\frac{3\,(1-v)}{E}\left(\frac{\sigma_0}{\beta v_f}\right)\left[\cosh\left(\frac{\sigma_e}{\sigma_0}\right)-1\right]-\frac{1}{n_D}\right\},\end{aligned} \tag{6}$$

where σ_0 is the reference stress $\sigma_0 = 2k_BT/\Omega$. Furthermore, the hydrostatic stress contribution $\dot{\varepsilon}_{ij}^{h}$ could be expressed as [21]

$$\dot{\varepsilon}_{ij}^{h} = \frac{(1-2v)\xi}{3E+(1-2v)\xi\sigma_{kk}}\dot{\sigma}_{kk}\,\delta_{ij}. \tag{7}$$

3. FEM Simulations

The above constitutive laws are then implemented into ABAQUS code [25] by using UMAT, which is developed to incorporate specific constitutive equations for individual materials. The details for the computational process could be obtained from reference [21]. Instead of the three-dimensional model, two-dimensional FEM is used in this work in order to reasonably capture the key deformation mechanism without costing much computational resources [15–17, 21]. In this framework, the strain localization is described by an internal state variable, i.e., the normalized free-volume v_f, as shown in equation (6). The evolution of strain localization could represent for the shear banding process. It means shear banding preferentially takes place at the regions where the higher density of free volume occurs. Besides, the plastic flow stress is a function of the effective Mises stress, the corresponding free volume as well as the hydrostatic stress. Therefore, all the variables such as stress and free volume could be calculated, updated, and stored in ABAQUS packages for the purpose of observations and analyses.

The specimen used for simulation is rectangular with the size of 3 mm × 6 mm, as shown in Figure 1. It comprises about 30000 ABAQUS CPS4R elements for the specimen without notches. In fact, a rectangular specimen in test should be at a status between plane stress and plane strain. In [7], the thickness is 3 mm, in terms of the height 6 mm and width 3 mm, and the stress status should be relatively closer to plane stress. Therefore, the plane stress element type was chosen for analysis. In this model, the bottom of the sample is fixed in loading direction while two ending points of the bottom line are not allowed to move in both x and y directions. The remaining nodes of the bottom line are free to move along x direction. On the contrary, continuous tensile or compressive displacement is applied on top of the sample. In a similar way, for the sample with notches, the same boundary conditions are employed in order to make a direct comparison among different samples. Loading rate is fixed at $10^{-6}\,s^{-1}$.

It is suggested that the initial free volume in sample distributes randomly which follows a Gaussian distribution. Therefore, in the FEM process, initial free volume should

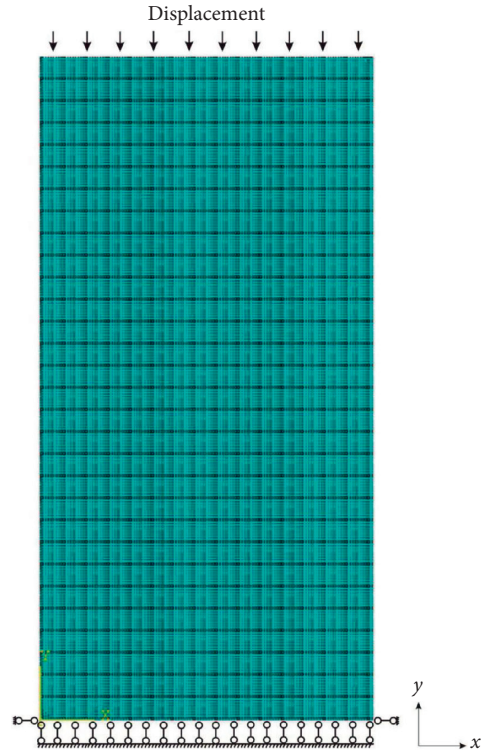

Figure 1: Boundary conditions on the specimen used in this work.

be assumed before calculation. Based on the work obtained by Chen et al. [26], the mathematical expression of the disturbance in the form of a two-dimensional Gaussian function could be displayed as [26]

$$v_{f0}(x,y) = v_0 + \delta\,\exp\left(-\frac{(x-x_0)^2}{\Delta_x^2}-\frac{(y-y_0)^2}{\Delta_y^2}\right). \tag{8}$$

In the above equation, the initial free volume v_0 is assumed to be 0.05; (x_0, y_0) is a random coordinate within the specimen region; δ is the amplitude of disturbance and presupposed to $v_0/10$; and Δ_x and Δ_y are the characteristic half widths [26].

4. Results and Discussion

4.1. Parameter Determination and Validations. Regarding the notch effect of metallic glasses, some systematic experiments have provided direct phenomenal evidences which could be used to validate our simulated results. Here, we borrowed the results in [7] to verify the reliability of current work. For the metallic glass $Zr_{52.5}Ni_{14.6}Al_{10}Cu_{17.9}Ti_5$ [7], its measured tensile and compressive strengths are 1.66 GPa and 1.84 GPa, respectively [27]. It demonstrates an obvious tensile and compressive asymmetry, and the compressive strength is higher than tensile strength, which is consistent with our previous description on hydrostatic stress. In this work, material parameters used in FEM could be achieved by comparing with the measured stress-strain relations continuously (as reported in [16, 17, 21]). In detail, the determination of those materials parameters is a manual

process in which the values of different parameters need to be input for trial until the computational and experimental curves match. After several attempts, the material properties for this metallic glass are $E = 96$ GPa, $\upsilon = 0.36$, $\xi = 0.1$, $n_D = 3$, $\alpha = 0.75$, and $\beta = 1$. $\xi = 0.1$ is the parameter which could reflect the hydrostatic stress contribution for metallic glass, and it is also a material-dependent coefficient [21].

Figure 2 plots the engineering stress-strain curves for this Zr-based metallic glass obtained by experiments [27] and simulations. From the simulated results, it can be seen that the patterns for both curves are very similar. After the stress reaches the highest stress, it exhibits an obvious softening behavior which is doubtless attributed to the shear banding localization. Furthermore, the yield strength under compression is slightly higher than that in tensile loading. The simulated compression strength is measured as 1.83 GPa while the strength under tension is 1.64 GPa. These results are very close to the experiment results in reference [27] (tensile and compressive strengths are 1.66 GPa and 1.84 GPa in experiment). It proves that the parameters determined above could result in acceptable precision and hydrostatic stress is indeed significant which could lead to tensile and compressive strength asymmetry.

In order to further understand the process of shear band evolution, Figures 3 and 4 display the contours of shear banding evolution under tension and compression, respectively. The color maps represent the free-volume distribution in equation (6), which can stand for the shear band evolution process via Mises plasticity criterion. Figure 3(a) shows the deformation patterns at the initial stage in which free volume are dispersed randomly within the samples. When strain ε is increased up to 2.49% (see Figure 3(c)), some short thin free-volume localization regions are formed, and the specimen is expected to slide along one shear band once the instability condition has been met [28]. Because there is no term in this model describing the instability process, the current simulation is not able to estimate when the specimen will fracture along one shear band finally. When strain ε is 5.0%, deformation patterns in Figure 3(d) show that multiple large shear bands are formed in sample and it is in agreement with the simulated results by Jiang [16]. On the contrary, the shear band evolution morphology under compressive loading is similar to that in under tension, as shown in Figures 4(a)–4(d). The only difference is the degree of free-volume localization. Taking Figures 3(d) and 4(d) for comparison, under the same strain level, the free volume concentration in tension is in the range of 0.0513~0.0830, which is slightly higher than that in compression (0.0489~0.0792). Although the difference between two cases is not pronounced, the difference on the tensile and compressive strength after computation could be noticeable according to the constitutive laws from equations (1)–(7). Besides, it could be understood by shrink effect induced by compressive hydrostatic stress which could suppress the expansion of free volume and delay its localization. It also explains why compressive strength is higher than tensile strength (see Figure 2).

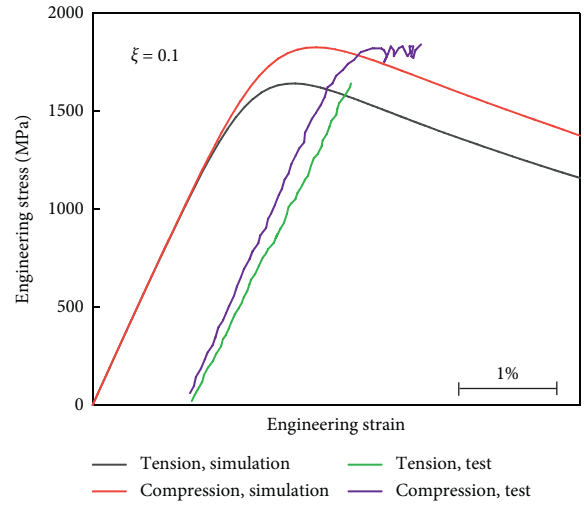

Figure 2: Simulated engineering stress-strain curves under tensile and compressive loadings, both simulation and test results [27].

In brief, comparison between experiments and simulations as well as the shear band evolution process confirms that the parameters being determined are reasonable to elucidate the asymmetry of tension and compression caused by hydrostatic stress.

4.2. Deformation Behavior of Notched and Unnotched Samples

4.2.1. Compressive Deformation Process for Notched Samples with Different Configuration. In [7], notch effect was systematically investigated, and it was found that the compressive plasticity of specimen could be enhanced largely when two symmetric notches were installed. Although this plasticity improvement has been revisited numerically by Jiang [16], there is no term delineating hydrostatic stress contribution in Jiang's work [16]. Therefore, it is necessary to elucidate the notch effect with the consideration of hydrostatic stress. Figure 5(a) replots four samples with different preset notches based on [7]. The dimension in these specimens strictly follows the sample configuration in Zhao et al. work [7]. The radius of notch or circular hole in Figure 5(a) is identically 0.5 mm. The size of all four samples are 3 mm × 6 mm. In specimen A, there is only one semicircular notch in the middle of one long edge. Specimen B contains two unsymmetric semicircular notches while a circular hole is constructed in specimen C. Specimen D consists of two symmetric semicircular notches which was found to have the highest plastic deformation ability among these four specimens [7].

After computation, engineering stress-strain curves could be obtained according to the data at different strain amplitudes. Here, the engineering stress-strain is defined as the ratio of all the forces applied on the top end to the minimum cross-section of specimen. For example, the minimum cross-section of specimen D is 2.0 mm instead of 3.0 mm. Then, Figure 5(b) shows the computed stress-strain curves for all the four samples. It is seen that the yield

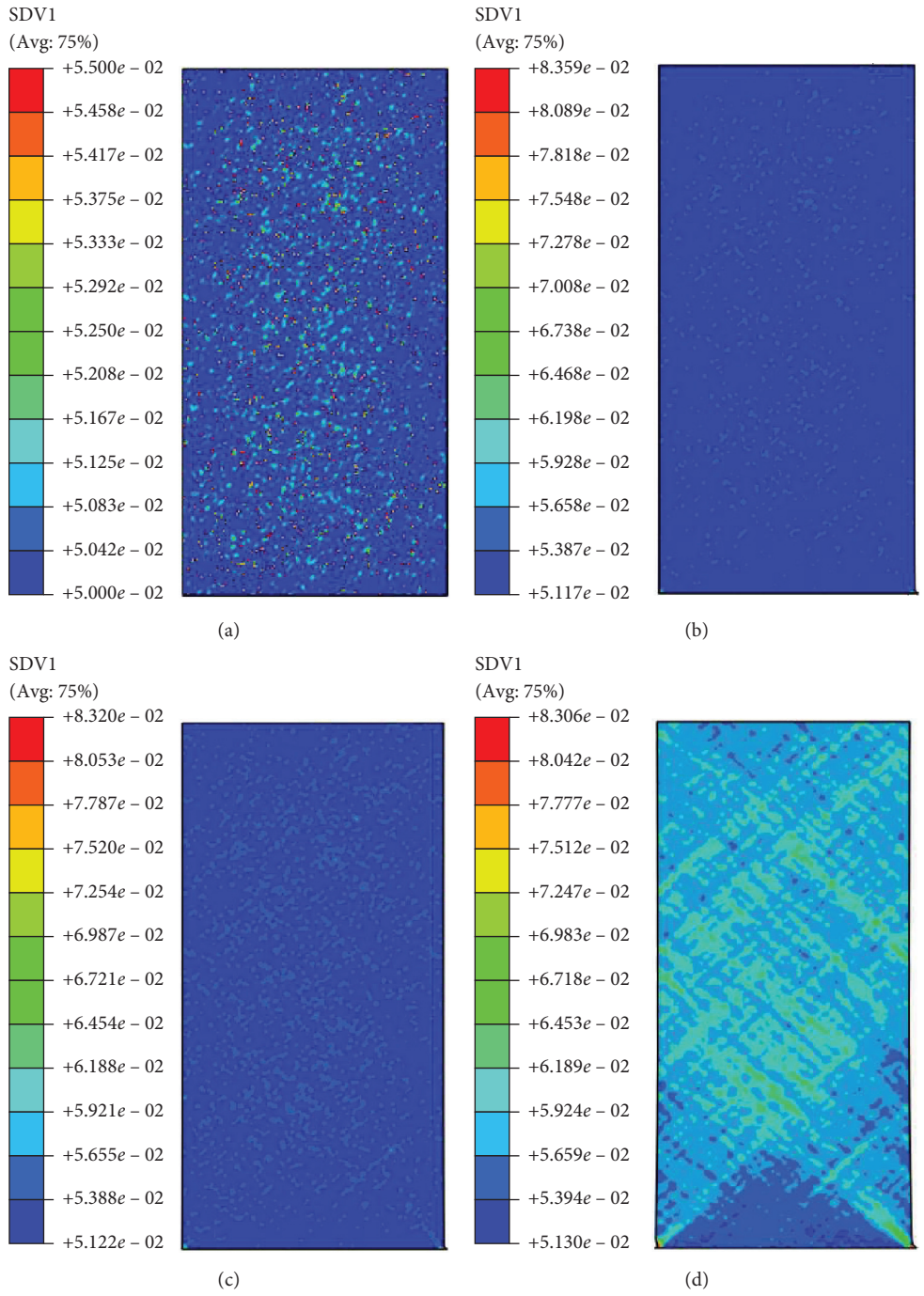

Figure 3: Contours plot of the shear banding evolution in the samples at different strains under tensile loading. (a) $\varepsilon = 0\%$; (b) $\varepsilon = 2.25\%$; (c) $\varepsilon = 2.48\%$; (d) $\varepsilon = 5.0\%$.

strength and plasticity of specimen D is distinctly higher than the others. The yield strength is 2.19 GPa, which is very close to the value found in experiment (2.24 GPa). It also shows that the yield strength for specimens A–C is almost the same, which is around 1.90 GPa. On the contrary, the elastic-plastic deformation duration in specimen D is also the longest, and it implies the highest plastic deformation process in specimen D. Furthermore, in order to better validate the reliability of present work, Figure 5(c) displays the comparison of yield strength for all the four samples with experimental results [7] as well as the simulated work in Jiang's work [16]. It could be clearly seen that a better agreement could be found by using the hydrostatic-stress included model, compared with the model without hydrostatic stress terms. It proves that the hydrostatic stress could not be negligible when the complex stress state is involved. It should be mentioned that the yield strength data used in Figure 5(c) have been converted into engineering

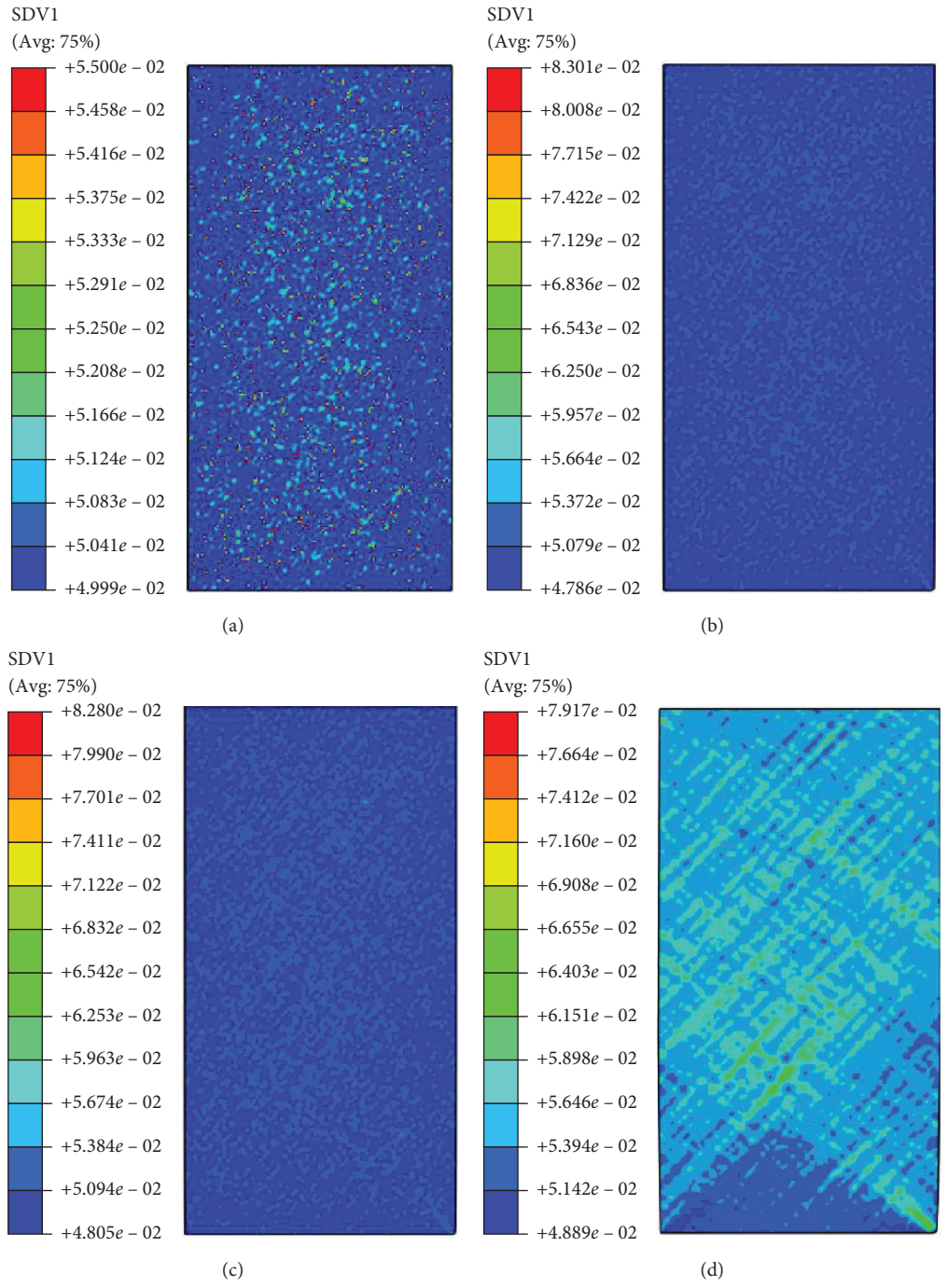

Figure 4: Contours plot of the shear banding evolution in the specimens at different strains under compressive loading. (a) $\varepsilon = 0\%$; (b) $\varepsilon = 2.29\%$; (c) $\varepsilon = 2.49\%$; (d) $\varepsilon = 5.0\%$.

stress. Besides, for specimen D (in Figure 5(a)), in both simulations and experiments, the maximum stresses were picked for comparison since monolithic metallic glass rarely displays work-hardening behavior like metal materials. Instead, once the stress reaches the yield strength (for most of cases, yield strength is close to the maximum stress), the specimen fractures right away. Actually, elastic and plastic models were considered in current work. The plastic deformation ability could be inferred by observing the stress-strain curve. Since there is no term of fracture criterion being considered in this work, the threshold at which the specimen is supposed to fracture cannot be determined by the present work. However, the different plastic abilities on those notched specimens could be reasonably reflected from the stress-strain curves.

In order to obtain the detailed microdeformation behavior, Figures 6(a)–6(f) show the shear banding evolution for specimens A–C which display poor plasticity. Figure 6(a)

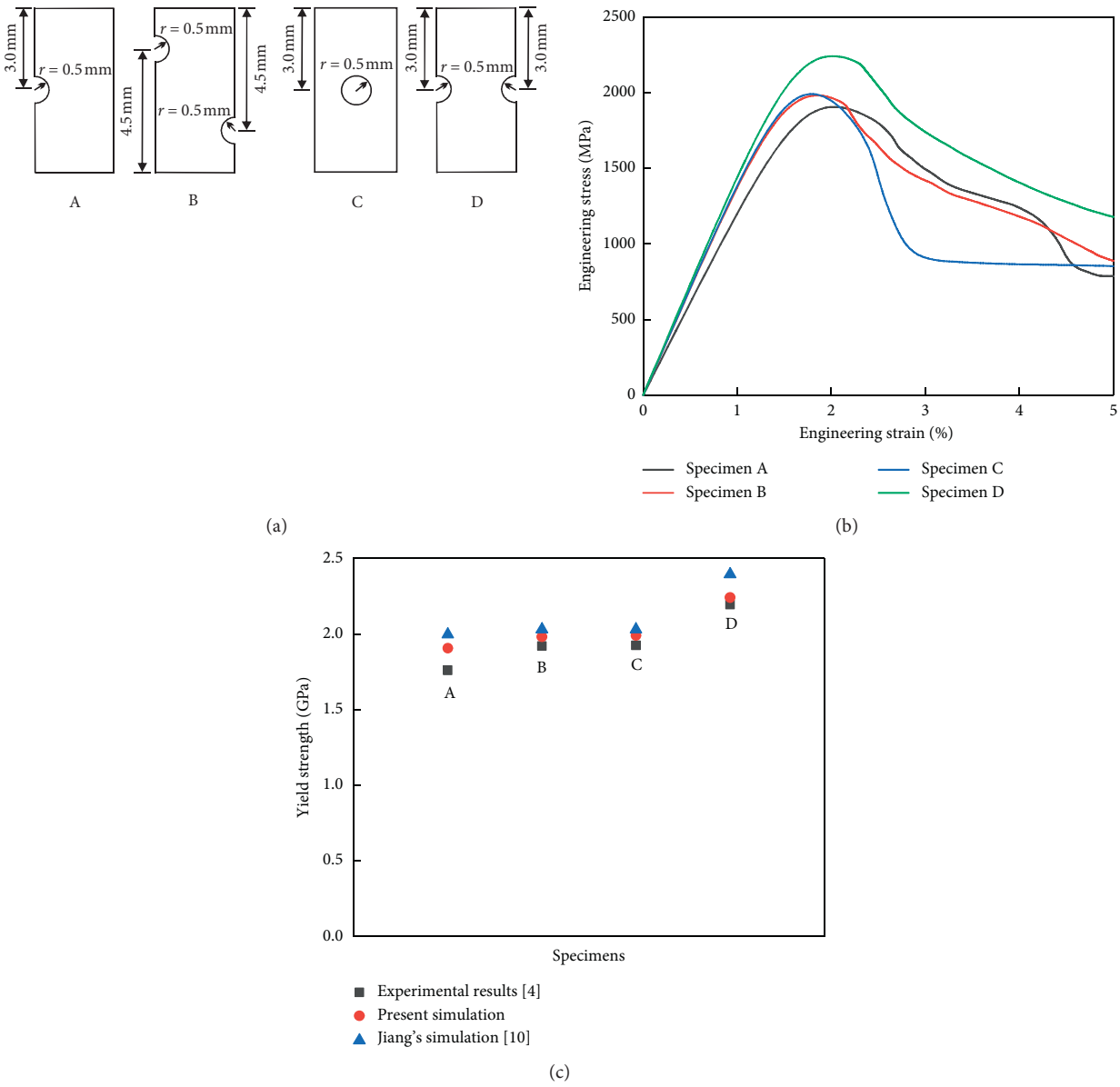

Figure 5: (a) Configuration of notched specimens [4]. (b) Engineering stress-strain curves for four notched specimens under compressive loading. (c) Comparison of yield strength for all the four notched specimens along with experimental results [7] and Jiang's simulation [16]. Obvious strength and plasticity improvement are found on sample with two symmetric notches (specimen D).

illustrates the free-volume distribution when strain ε is 2.02%, and it is found that the free-volume concentrates around the notch region and is about to propagate towards the inner part of specimen. When strain ε is increased to 2.38%, an obvious region with higher density of free volume is formed, demonstrating the shear banding tendency and direction. It could be speculated that the specimen might fracture along one major shear band once the instability conditions are reached. For the specimen with two unsymmetric notches (in Figures 6(c) and 6(d)), the shear band initiates from the notch region and expands into the internal region of the sample (see Figure 6(c)). Finally, the sample is expected to failure along the major shear band formed between two notches, as shown in Figure 6(d). It is also consistent with the experimental finding in [7]. Besides, Figures 6(e) and 6(f) illustrate the results for specimen with one circular hole in the middle. According to the free-volume patterns, the sample may fracture along one inclined shear band finally, which is in agreement with the observation in tests [7].

Different from specimens A–C, sample D exhibits a higher strength and plasticity based on stress-strain curves in Figure 5(b). It must be corresponding to the shear banding evolution during deformation process. Then, Figures 7(a)–7(c) display the free-volume concentration features under different strains. When strain ε is relatively low at 1.44% (in Figure 7(a)), intense free volume is located at the notch region. When ε

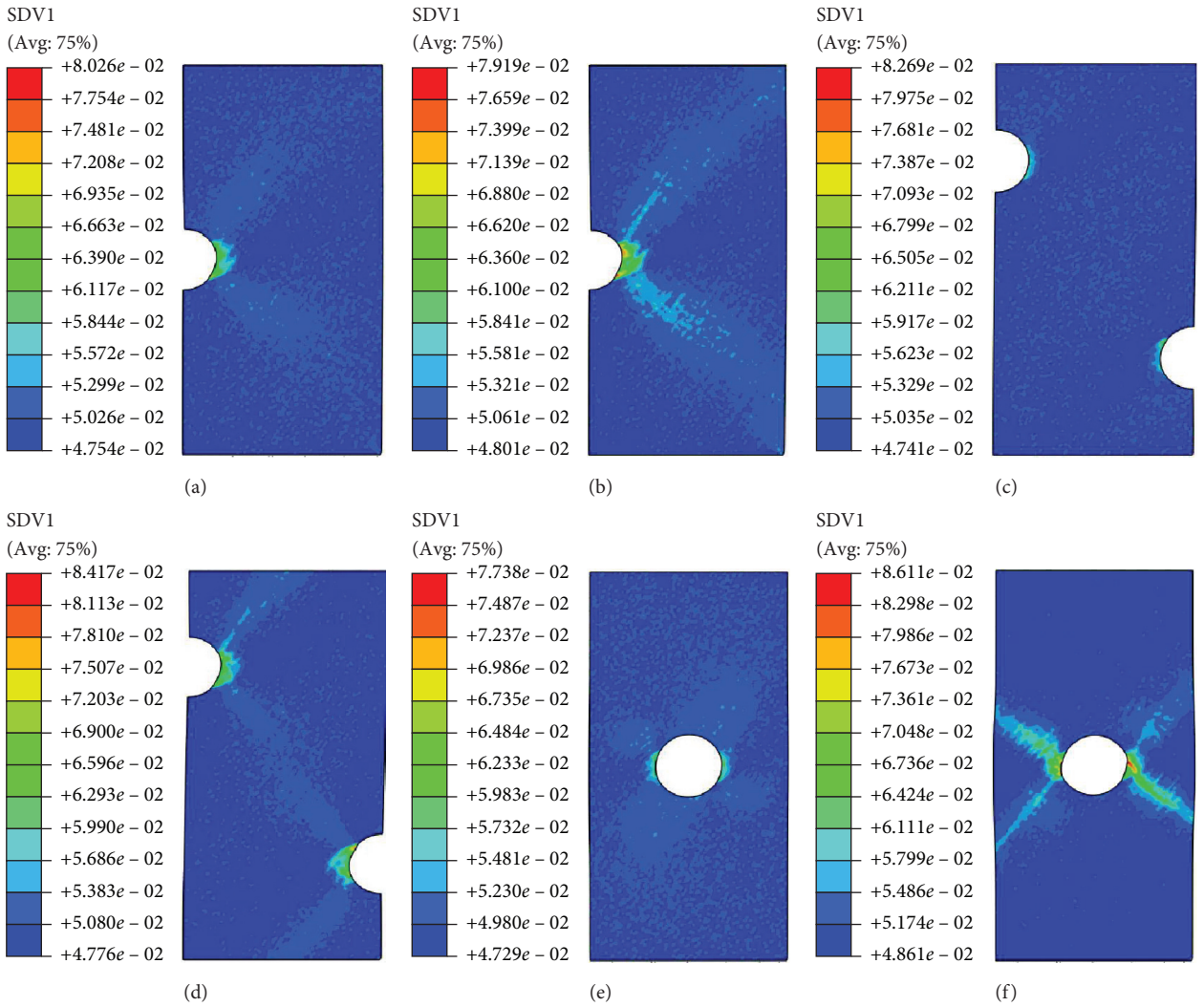

Figure 6: Contour plots of free-volume evolution for specimens A–C under different compressive strain levels. (a) Specimen A $\varepsilon = 2.02\%$. (b) Specimen A $\varepsilon = 2.38\%$. (c) Specimen B $\varepsilon = 1.47\%$. (d) Specimen B $\varepsilon = 2.05\%$. (e) Specimen C $\varepsilon = 1.56\%$. (f) Specimen C $\varepsilon = 2.31\%$.

is up to 2.08% shown in Figure 7(b), two vague V-shaped regions are formed within the sample. The pattern is highly coincident with the experimental observation [7]. With an even higher strain ε 5.0%, a clear intersection of two shear bands is seen in sample. This intersection should be responsible for the high strength enhancement found in both simulations and experiments [7]. Besides, it could postpone the sample from rapidly fracturing along one major shear band. It again proves the reliability of the present work.

4.2.2. Asymmetry between Tension and Compression for Notched Specimens. As stated above, the existence of hydrostatic stress could suppress the onset of free-volume and the following shear band propagation, resulting in a higher compressive yield strength than that under tension for smooth specimen [21, 27]. Therefore, it is necessary to make predictions on samples under tension so as to understand the hydrostatic stress effect of notched samples since this has not been investigated yet up to now. Although numerical investigation has been performed by Jiang [16] on notched metallic glasses, it has no terms accounting for hydrostatic stress so that no asymmetry between tension and compression could be achieved by that model [16]. For the sake of demonstrating the asymmetry between tension and compression for notched specimens, Figure 8(a) plots the tensile engineering stress-strain curves for the four sample A–D (in Figure 5(a)). Generally, yield strengths under tension are obviously lower than those under compression, compared with Figure 5(b). Moreover, it is clearly shown that the mechanical responses induced by unsymmetric notches are quite similar, illustrated in specimens A–C. For these three samples, the tensile yield strengths are very comparable which is consistent with the results under compression in Figure 5(b). However, for specimen D, because of the symmetric notches, the yield strength of specimen D is higher than the other three samples.

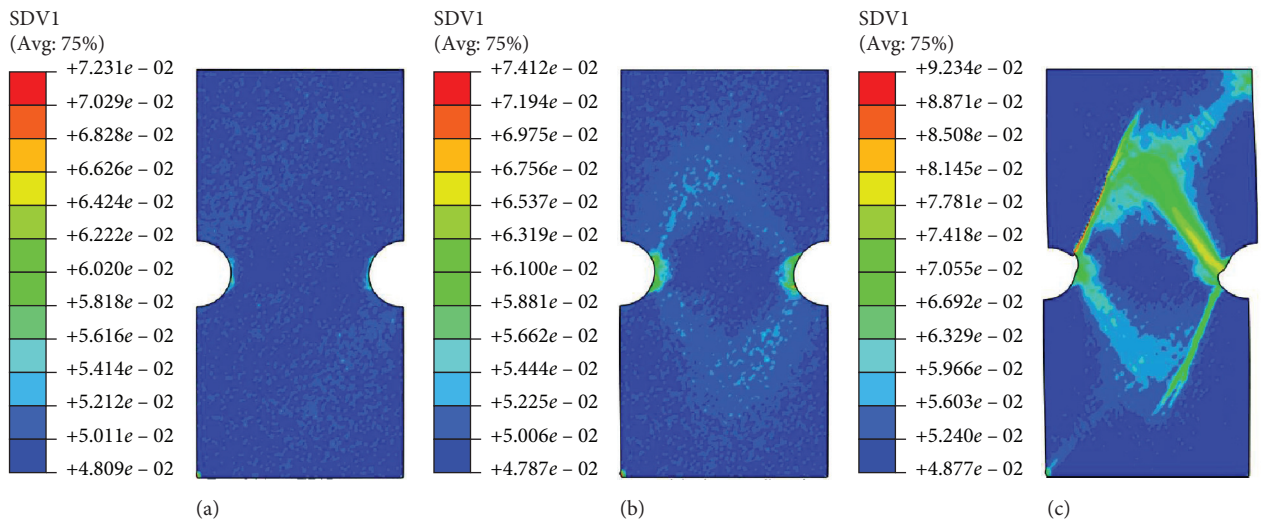

Figure 7: Shear banding illustration of free-volume localization for specimen D under different compressive strain levels. (a) $\varepsilon = 1.44\%$; (b) $\varepsilon = 2.08\%$; (c) $\varepsilon = 5.0\%$.

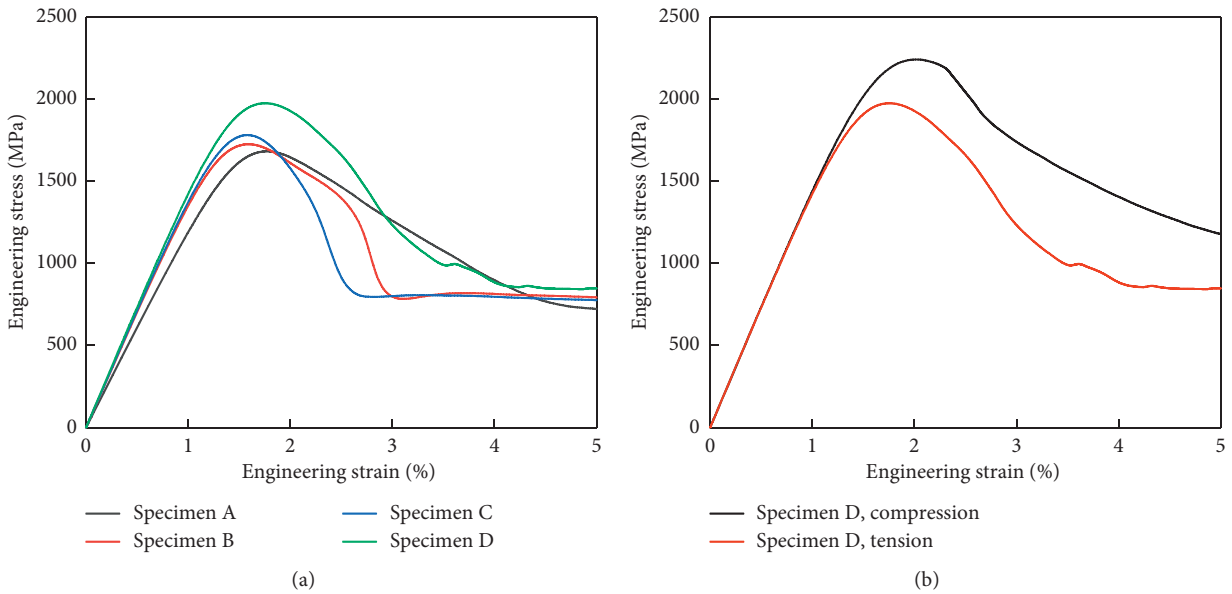

Figure 8: (a) Engineering stress-strain curves for specimens A–D under tensile loadings. (b) Comparison of simulations on specimen D in both tension and compression.

It could be explained that the shear band entanglement caused by two symmetric notches may hinder the fast propagation of shear bands and lead to an improvement of yield strength and plasticity even under tensile loadings [8]. Besides, Figure 8(b) shows the comparison of simulations for specimen D in both tension and compression. Higher strength and larger plasticity are found in compression. The difference between tension and compression on specimen D could also be obtained numerically.

On the contrary, Figures 9(a)–9(c) show the shear band evolution by the free-volume location contour plot. Although the shear band interaction is also found in Figure 9(c), a large plasticity is not expected to happen since the tensile stress will make specimen fracture right away once instability starts. Furthermore, Figure 10 illustrates the comparison on yield strengths under compression and tension. Wherein, the compressive strength is accordingly higher than tensile strength. It proves again that the compressive hydrostatic stress rather than tensile hydrostatic stress could confine the initiation of shear bands under complex stress states and give rise to asymmetry of tension and compression for notched samples.

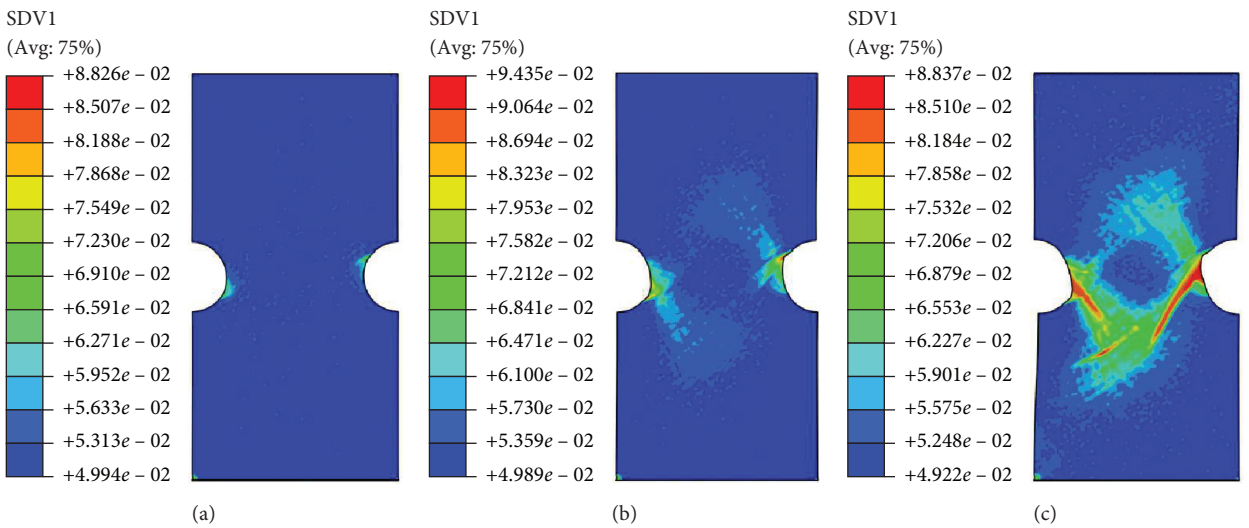

Figure 9: Shear banding illustration for specimen D under different tensile strain levels. (a) $\varepsilon = 1.35\%$; (b) $\varepsilon = 2.15\%$; (c) $\varepsilon = 3.02\%$.

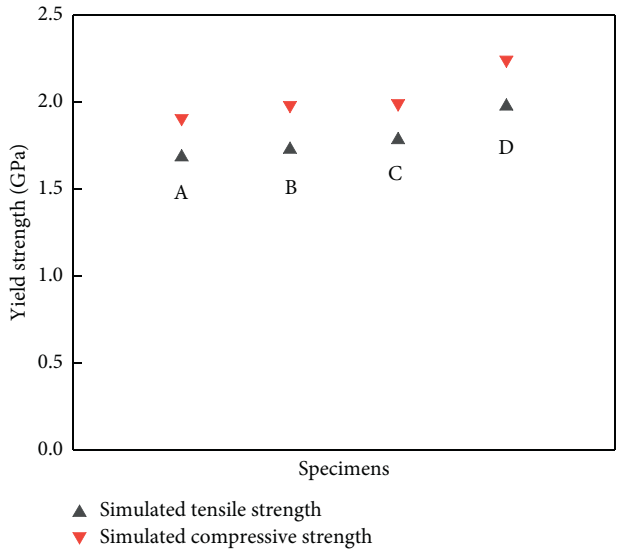

Figure 10: Comparison on the yield strength between tension and compression. It is found that compressive yield strengths are uniformly higher than ones under tension because of hydrostatic stress effect.

4.3. Effect of Aspect Ratio on the Deformation of Notched Samples. As researched before [16, 29, 30], the aspect ratio of the specimen could somehow change the plastic deformation of metallic glasses due to the different geometrical configuration. In the following, the effect of the aspect ratio on specimen with two symmetric notches is carried out numerically to reveal the mechanical responses by considering hydrostatic stress terms into the predictive model. Figure 11(a) displays the geometrical settings of four samples E–H with the aspect ratio from 1.0 to 2.0. By taking compression, for example, Figure 11(b) shows the compressive engineering curves for specimen E–H. In general, it is seen that the yield strength increases with higher value of aspect ratio H/a. This trend is also consistent with the simulation in Jiang's work [16]. Besides, uniform elongation is used to characterize the stable deformation stage for those samples. Hereby, the uniform elongation is defined as the total strain including the elastic and plastic strain till the occurrence of maximum stress. Here, we just borrowed the uniform elongation of metal materials to characterize the plastic deformation behavior. The corresponding values are therefore shown in Figure 12. Along with the increment of the aspect ratio, uniform elongation exhibits a slight climbing tendency in the first stage and then drops down afterwards. This character is in agreement with the rule found in Jiang's work [16]. It elucidates that the aspect ratio does have influence on plastic deformation process when hydrostatic stress is included.

4.4. Discussion. Figure 13 shows the hydrostatic stress distribution for five different samples including smooth and notched specimens under tensile loading. It could be found that the notch has redistributed the stress distribution which results in different patterns of hydrostatic stress. Therefore, it is necessary to incorporate the hydrostatic stress term to investigate the notch effect. The above numerical results elucidate that hydrostatic stress is the key to influencing the strength asymmetry between tension and compression for samples with different notches. Simulations demonstrate that the high strength and plasticity for the specimen with two symmetric notches is attributed to the shear band intersection being formed during free-volume evolution. The emphasis of this work is to show the hydrostatic stress effect on the notched specimens. As shown in Figure 5(c), by incorporating the hydrostatic stress term into free-volume theory, the simulated results are closer to the experimental

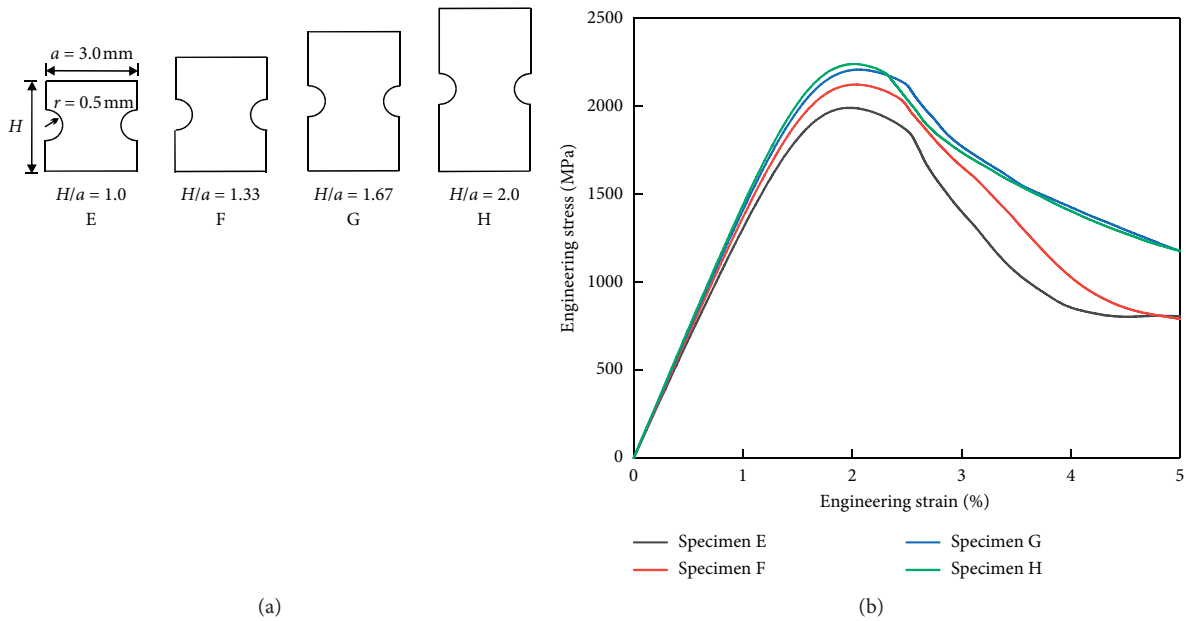

Figure 11: (a) Configuration of notched samples with different aspect ratios H/a from 1.0 to 2.0, marked as specimens E–H. (b) Compressive engineering stress-strain curves for samples E–H.

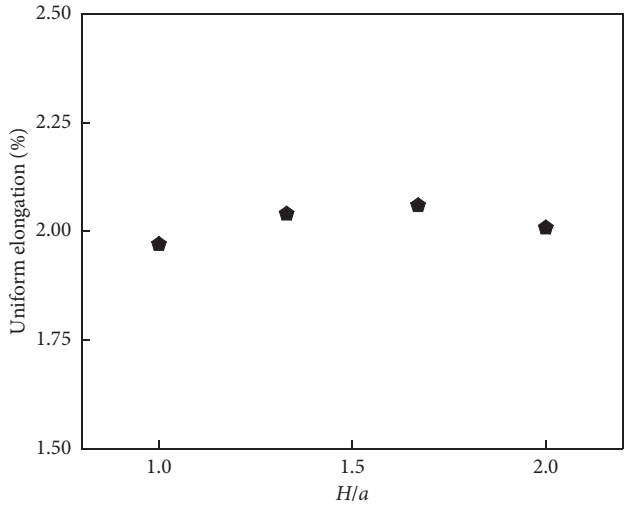

Figure 12: Dependence of uniform elongation for specimens with different aspect ratios H/a.

results, compared with the work conducted by Jiang [16]. In Jiang's work [16], the strength asymmetry could not be obtained on notched samples because of the lack of hydrostatic stress in the constitutive laws. It also reflects the difference of the hydrostatic-stress-free model (Jiang's work [16]) and hydrostatic-stress-related work (current research). Compared with the rod specimens, the hydrostatic stress is much smaller in plate specimens, it will be even better to investigate the effect of hydrostatic stress on strength by changing the dimension of notch. However, in terms of the length limit of this paper, it will be performed in the next step.

Besides, the current simulations are also different from other related simulations such as Li et al. [31, 32], in which there are no hydrostatic stress terms incorporated into the free volume evolution equation. It is hoped that this work could function as a useful supplement to the existing numerical investigations on metallic glasses.

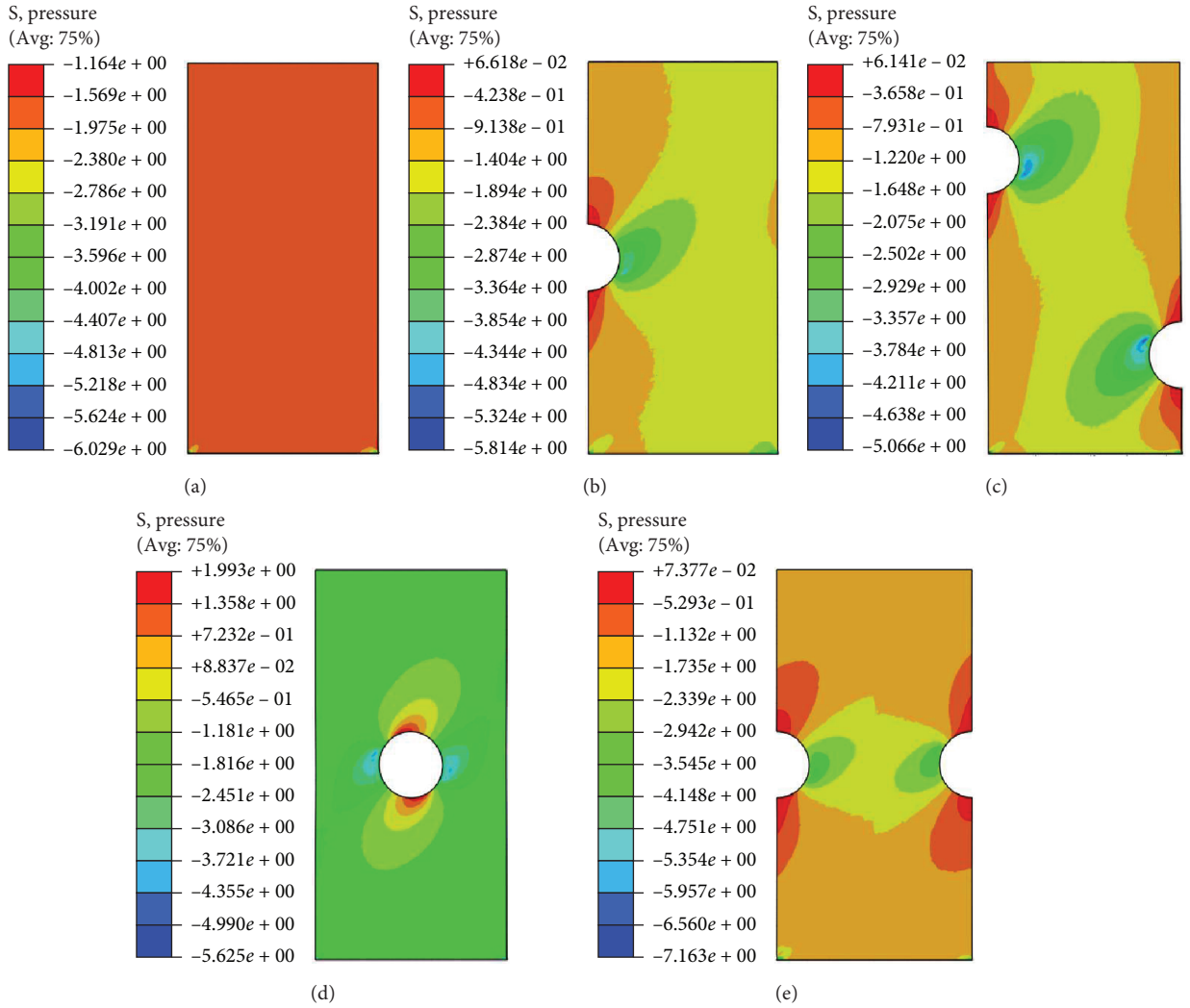

FIGURE 13: Hydrostatic stress distribution (described by "pressure" in ABAQUS) for five samples in tension. (a) $\varepsilon = 1.0\%$, smooth specimen; (b) $\varepsilon = 1.0\%$, specimen A; (c) $\varepsilon = 1.0\%$, specimen B; (d) $\varepsilon = 1.0\%$, specimen C; (e) $\varepsilon = 1.0\%$, specimen D, in which, the unit of pressure is actually denoted as $\sigma_{\text{hydrostatic}}/\sigma_0$ in which σ_0 is 225 MPa (according to the deduction process in [15]).

5. Conclusions

This work performed a numerical study on notch effect of metallic glass by a revised free-volume theory considering hydrostatic stress. Conclusions could be drawn as below:

(1) For the samples without notches, a good agreement could be obtained between the present simulations and previous experimental results, and this model could reasonably describe the strength asymmetry between tension and compression [21]. For notched specimens, compressive yield strengths obtained by the present model are very close to the experimental values obtained by Zhao et al. [7]. Besides, the simulated stress-strain curves on the four notched sample demonstrate that the sample with two symmetric notches exhibits a higher strength and larger plasticity, compared with other specimens. Contour plots on free-volume evolution show that the higher strength and plasticity for specimen with two symmetric notches is attributed to the intersection of two major shear bands during deformation process.

(2) Asymmetry between tension and compression was found by comparing the simulated results under tension and compression for notched samples. For the same geometrical configuration, tensile yield strength is lower than the corresponding compressive yield strength because of shrink effect induced by compressive hydrostatic stress.

(3) Simulations demonstrated that the aspect ratio has a slight impact on the plastic deformation behavior of samples with two symmetric notches, when hydrostatic stress is considered in the model.

Data Availability

The data used to support the findings of this study are included within the article.

Conflicts of Interest

The authors declare that they have no conflicts of interest.

Acknowledgments

The work was financially supported by the National Natural Science Foundation of China (NSFC) (Grant no. 5167052181).

References

[1] A. Inoue, B. Shen, H. Koshiba, H. Kato, and A. R. Yavari, "Cobalt-based bulk glassy alloy with ultrahigh strength and soft magnetic properties," *Nature Materials*, vol. 2, no. 10, pp. 661–663, 2003.

[2] W. L. Johnson, "Bulk glass-forming metallic alloys: science and technology," *MRS Bulletin*, vol. 24, no. 10, pp. 42–56, 1999.

[3] H. Jia, G. Wang, S. Chen, Y. Gao, W. Li, and P. K. Liaw, "Fatigue and fracture behavior of bulk metallic glasses and their composites," *Progress in Materials Science*, vol. 98, pp. 168–248, 2018.

[4] A. L. Greer, Y. Q. Cheng, and E. Ma, "Shear bands in metallic glasses," *Materials Science and Engineering: R: Reports*, vol. 74, no. 4, pp. 71–132, 2013.

[5] J. C. Qiao, Q. Wang, J. M. Pelletier et al., "Structural heterogeneities and mechanical behavior of amorphous alloys," *Progress in Materials Science*, vol. 104, pp. 250–329, 2019.

[6] N. Wang, J. Ding, F. Yan, M. Asta, R. O. Ritchie, and L. Li, "Spatial correlation of elastic heterogeneity tunes the deformation behavior of metallic glasses," *Npj Computational Materials*, vol. 4, no. 1, 2018.

[7] J. X. Zhao, F. F. Wu, R. T. Qu, S. X. Li, and Z. F. Zhang, "Plastic deformability of metallic glass by artificial macroscopic notches," *Acta Materialia*, vol. 58, no. 16, pp. 5420–5432, 2010.

[8] R. T. Qu, J. X. Zhao, M. Stoica, J. Eckert, and Z. F. Zhang, "Macroscopic tensile plasticity of bulk metallic glass through designed artificial defects," *Materials Science and Engineering: A*, vol. 534, pp. 365–373, 2012.

[9] S. H. Chen, K. C. Chan, and L. Xia, "Effect of stress gradient on the deformation behavior of a bulk metallic glass under uniaxial tension," *Materials Science and Engineering: A*, vol. 574, pp. 262–265, 2013.

[10] S. H. Chen, K. C. Chan, and L. Xia, "Deformation behavior of a Zr-based bulk metallic glass under a complex stress state," *Intermetallics*, vol. 43, pp. 38–44, 2013.

[11] K. M. Flores and R. H. Dauskardt, "Mean stress effects on flow localization and failure in a bulk metallic glass," *Acta Materialia*, vol. 49, no. 13, pp. 2527–2537, 2001.

[12] Z. D. Sha, Q. X. Pei, V. Sorkin, P. S. Branicio, Y. W. Zhang, and H. J. Gao, "On the notch sensitivity of CuZr metallic glasses," *Applied Physics Letters*, vol. 103, Article ID 081903, 2013.

[13] J. Pan, H. F. Zhou, Z. T. Wang, Y. Li, and H. J. Gao, "Origin of anomalous inverse notch effect in bulk metallic glasses," *Journal of the Mechanics and Physics of Solids*, vol. 84, pp. 85–94, 2015.

[14] F. Spaepen, "A microscopic mechanism for steady state inhomogenous flow in metallic glasses," *Acta Metallurgica*, vol. 25, pp. 405–415, 1977.

[15] Y. F. Gao, "An implicit finite element method for simulating inhomogeneous deformation and shear bands of amorphous alloys based on the free-volume model," *Modelling and Simulation in Materials Science and Engineering*, vol. 14, no. 8, pp. 1329–1345, 2006.

[16] Y. Jiang, "Numerical study of the notch effect on the malleability of bulk metallic glasses based on the free-volume theory," *Journal of Materials Research*, vol. 31, no. 6, pp. 765–774, 2016.

[17] Y. Jiang, "Effect of testing conditions on the compressive plasticity of bulk metallic glasses," *Journal of Materials Research*, vol. 31, no. 17, pp. 2686–2694, 2016.

[18] P. Thamburaja and R. Ekambaram, "Coupled thermo-mechanical modelling of bulk-metallic glasses: theory, finite-element simulations and experimental verification," *Journal of the Mechanics and Physics of Solids*, vol. 55, no. 6, pp. 1236–1273, 2007.

[19] P. Thamburaja, "Length scale effects on the shear localization process in metallic glasses: a theoretical and computational study," *Journal of the Mechanics and Physics of Solids*, vol. 59, no. 8, pp. 1552–1575, 2011.

[20] W. Rao, J. Zhang, and G. Z. Kang, "A-micromechanical model for the grain size dependent super-elasticity degeneration of NiTi shape memory alloys," *Mechanics of Materials*, vol. 125, pp. 52–69, 2018.

[21] J. X. Zhao, Y. Jiang, L. Y. Geng, and J. M. Gong, "On the effect of hydrostatic stress on plastic deformation in metallic glasses," *Journal of Non-Crystalline Solids*, vol. 521, Article ID 119485, 2019.

[22] M. K. Shete, T. Dutta, I. Singh, R. Narasimhan, and U. Ramamurty, "Tensile stress-strain response of metallic glass matrix composites reinforced with crystalline dendrites: role of dendrite morphology," *Intermetallics*, vol. 83, pp. 70–82, 2017.

[23] Z. F. Zhang, J. Eckert, and L. Schultz, "Difference in compressive and tensile fracture mechanisms of $Zr_{59}Cu_{20}Al_{10}Ni_8Ti_3$ bulk metallic glass," *Acta Materialia*, vol. 51, no. 4, pp. 1167–1179, 2003.

[24] R. Huang, Z. Suo, J. H. Prevost, and W. D. Nix, "Inhomogeneous deformation in metallic glasses," *Journal of the Mechanics and Physics of Solids*, vol. 50, no. 5, pp. 1011–1027, 2002.

[25] Simula Inc., *Abaqus Reference Manuals*, Simula Inc., Phoenix, AZ, USA, 2009.

[26] Y. Chen, M. Jiang, and L. Dai, "How does the initial free volume distribution affect shear band formation in metallic glass?" *Science China Physics, Mechanics and Astronomy*, vol. 54, no. 8, pp. 1488–1494, 2011.

[27] R. T. Qu, J. Eckert, and Z. F. Zhang, "Tensile fracture criterion of metallic glass," *Journal of Applied Physics*, vol. 109, no. 8, Article ID 083544, 2011.

[28] Z. Han, W. F. Wu, Y. Li, Y. J. Wei, and H. J. Gao, "An instability index of shear band for plasticity in metallic glasses," *Acta Materialia*, vol. 57, no. 5, pp. 1367–1372, 2009.

[29] S. Feng, G. Li, P. Yu et al., "Effects of aspect ratio on the shear band arrangements of Zr-based metallic glasses," *Metallurgical and Materials Transactions A*, vol. 46, no. 3, pp. 1119–1124, 2015.

[30] J. X. Zhao, R. T. Qu, F. F. Wu, S. X. Li, and Z. F. Zhang, "Deformation behavior and enhanced plasticity of Ti-based metallic glasses with notches," *Philosophical Magazine*, vol. 90, no. 29, pp. 3867–3877, 2010.

[31] W. D. Li, Y. F. Gao, and H. B. Bei, "Instability analysis and free volume simulations of shear band directions and arrangements in notched metallic glasses," *Scientific Reports*, vol. 6, no. 1, Article ID 34878, 2016.

[32] W. Li, H. Bei, and Y. Gao, "Effects of geometric factors and shear band patterns on notch sensitivity in bulk metallic glasses," *Intermetallics*, vol. 79, pp. 12–19, 2016.